Transp Porous Med (2012) 92:259–275
DOI 10.1007/s11242-011-9900-0

Unsteady Two-Dimensional Blood Flow in Porous Artery with Multi-Irregular Stenoses

Obaid Ullah Mehmood · Norzieha Mustapha · Sharidan Shafie

Received: 20 May 2011 / Accepted: 15 October 2011 / Published online: 1 November 2011

Abstract The flow characteristics of an unsteady axisymmetric two-dimensional (2D) blood flow in a diseased porous arterial segment with flexible walls are investigated. The arterial walls mimic the irregular constrictions whereas the lumen containing the thrombus, cholesterol, and fatty plaques represents the porous medium. The governing equations with appropriate initial and boundary conditions are solved numerically using MAC method. The discretization is done on staggered grid with non-uniform grid size and pressure-poisson equation is solved following SOR method. The pressure and velocity corrections are made cyclically until the steady state is achieved. It is observed that for decreasing permeability, flow is highly decelerated while pressure drop and wall shear stress increases. The separation zones and re-circulation regions are found for severe stenoses. Flow separation and re-circulation diminishes for decreasing permeability of the porous medium. Comparisons are provided with published experimental and numerical results.

Keywords Blood flow · Porous medium · MAC method · Flow separation · Multi-irregular stenoses

1 Introduction

The atheromal reduction of atherosclerotic lesions up to a critical limit disturbing the normal blood flow in the human arterial system is the main cause (Nerem and Seed 1972; Liepsch 2002) of many cardiovascular diseases resulting in cerebral infarction, myocardial infarction, cardiac arrest, epilepsy, and others. The occlusion in the artery called stenoses is due to the deposition of carbohydrates, fibrous tissues, and fats in the lumen. Initially, Young (1968) and then other researchers (Srivastava and Saxena 1997; Sud and Sekhon 1987; Srivastava et al. 2010; Mekheimer and Kot 2008) made efforts for the analytical treatment of the flow around

O. U. Mehmood · N. Mustapha (✉) · S. Shafie
Department of Mathematics, Faculty of Science, Universiti Teknologi Malaysia, 81310, Skudai, Johor, Malaysia
e-mail: norzieha@utm.my

the smooth stenoses. However, smooth stenoses is not suitable in real situations because the constriction in the arterial segment is highly irregular in nature as evident from the experimental study of Back et al. (1984). Keeping this fact in mind (Johnston and Kilpatrick 1991; Yakhot et al. 2005; Andersson et al. 2000; Mustapha et al. 2010; Jeong and Rhee 2009) considered irregular arterial constriction with valleys and ridges, in their investigations for blood flow.

The physiological domain for blood flow particularly in some pathological cases and blood diseases like thrombosis (formation of blood clots inside the lumen obstructing the flow), polycythemia or erythrocytoses, and other microangiopathic diseases refers to the blood flow in porous medium. Blood flow in the excess of fats, cholesterol plaques and blood clots (Dash et al. 1996; El-Shahed 2003), blood flow in kidneys, lungs, and small capillaries presents best examples for porous medium. Also biological tissues containing dispersed cells separated by voids, blood enters these tissues through arteries and perfuse into the tissue cells via blood capillaries which serves as porous medium (Khaled and Vafai 2003). Khaled and Vafai (2003) also suggested that the transport models through porous media are widely applicable to the simulation of blood flow across the tumor. The growth of tumor and its response to therapy are determined by transport of diffusive drugs to cancer cells and by their blood supply. Baish et al. (1997) considered the blood flow through a network of permeable vessel in an isotopic porous medium using Darcy law (1856). Lei et al. (1998) investigated the transvascular and extravascular transport of both fluid and macromolecules in a spherical solid tumor considering microvascular lymphatics and tissue space as porous medium. Their study and Milosevic et al. (1999) revealed that interstitial pressure was a major barrier in the macromolecular drug penetration in tumor.

The influence of geometrical features on hemodynamics and the impact of arterial wall layers on transport phenomenon and wall shear stress are imperative in study of porous media. Yang and Vafai (2006) presented a model for the low-density lipoprotein (LDL) transport in homogeneous porous four layered arterial wall coupled with blood flow in lumen. The permeability of each layer of arterial wall and osmotic pressure are characterized by the Staverman filtration and osmotic reflection coefficient. They concluded that pressure-induced increase of endothelial diffusive permeability and pressure-associated convective flow are responsible for the enhanced LDL uptake at higher transmural pressure which is susceptible for the increase of atherosclerosis in the presence of hypertension. Filtration velocity and LDL concentration profiles are dependent on different boundary conditions. Pulsatile flow plays a minor role in LDL transport within artery. Again for the same model (Yang and Vafai 2008) obtained the analytical solution based on primary transport in lateral direction. Analytical solutions are compared with numerical solutions and found better in estimation of LDL transport in straight geometry. A study of coupled macromolecule transport in blood stream and arterial wall is presented by Ai and Vafai (2006). They concluded that hypertension is the main cause for increase in transmural filtration and concentration polarization at lumen–endothelium interface. The maximum shear rate reaches its maxima before and velocity reaches its maxima after the constriction. The wall concentration shoots in stenosed region and dies out after the constriction.

Khakpour and Vafai (2008b) conducted the first geometrical gender-based study on the coupled blood flow and macromolecular transport phenomenon within the lumen and macroscopic homogeneous porous four layered arterial wall of the asymmetric aorta-iliac bifurcation. For selective permeability of each porous layer they introduced the Staverman filtration coefficient. They found that higher concentration of macromolecules such as LDL at the lumen–endothelium interface, different radius of curvature, take off angle, and the bifurcation points play vital role in the development of atherosclerosis. With constant endothelial

properties the concentration decreases up to 0.5% in recirculation region and in females, higher shear stress at aorta-iliac bifurcation is reported. Both shear stress and macromolecular concentration profiles are greatly affected by asymmetry and found uniform in males. Critical assessment of the several arterial transport models involving the study of fluid flow and mass transfer within the arteries highlighting the role of porous media was carried out by Khakpour and Vafai (2008a). Based on the arterial anatomy and related transport processes these models are classified into wall free, homogeneous wall, and multilayer wall model. The authors highlighted the three main challenges in modeling the arterial transport, they are: the accurate description of the artery, proper set of governing equations, and appropriate choice of boundary conditions. Three models are analyzed and multilayer model is given preference because it describes the arterial anatomy accurately. Authors also reported that these models do not include selective permeability for each porous layer and the osmotic pressure. To overcome this flaw, they suggested the incorporation of Staverman filtration and osmotic reflection coefficients as discussed by Yang and Vafai (2006) and Ai and Vafai (2006).

Dash et al. (1996) using Brinkman model investigated the pathological blood flow in porous medium by taking constant and radially varying permeability. The porous medium contains the accumulation of fatty plaques of cholesterol and artery-clogging blood clots in the lumen of the artery. They solved the governing equations for casson fluid model and concluded that the frictional resistance increases while flow rate decreases with decreasing permeability. Multilayer model (Khakpour and Vafai 2008a) best describes the arterial anatomy but the present model particularly represents the blood flow in diseased artery when the lumen contains the thrombus (blood clot), cholesterol, and fatty plaques depicting the lumen a porous media. The continuous accumulation of these substances near the intima gives rise to the constrictions and once the mild stenoses is generated; the resulting flow increases the disease evidently (Liepsch 2002). This attempt is devoted to study the effects of permeability on blood flow in a constricted porous-diseased arterial segment. The further assumptions taken into account are unsteadiness, flexibility of wall, couple of irregular stenoses, and the inlet boundary condition derived for porous medium (El-Shahed 2003). The MAC method given by Harlow and Welch (1965) and Welch et al. (1966) is adopted for the numerical simulation of governing equations in cylindrical coordinates.

2 Governing Equations

Consider the unsteady 2D incompressible viscous blood flow in the circular porous stenosed artery (Fig. 1). The blood flow is taken axisymmetric and fully developed in the arterial segment with couple of mild stenoses with 48% areal occlusion. The geometrical shape of the stenoses is irregular, presenting actual surface irregularities, taken from a main coronary

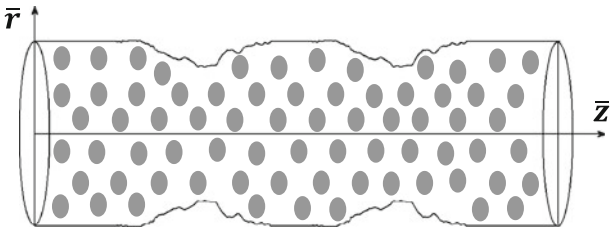

Fig. 1 Schematic diagram of porous artery with multiple stenoses

artery of human cadaver developed by Back et al. (1984). The time-dependent geometry of the stenoses is given by

$$\bar{R}\left(\bar{z},\bar{t}\right)=\left\{1+k_R\cos\left(\omega\bar{t}-\phi\right)\right\}\bar{R}(\bar{z}), \tag{1}$$

where $\bar{R}(\bar{z})$ is the radius of the constricted region taken from the data developed by Back et al. (1984), k_R is a constant, $\omega=2\pi f_{\mathrm{p}}$ is the angular frequency with f_{p} the pulse frequency and ϕ is the phase difference.

The mathematical model for considered blood rheology is based on the mass and momentum balances given by

$$\mathrm{div}\left(\mathbf{V}\right)=0, \tag{2}$$

$$\rho\frac{D\mathbf{V}}{D\bar{t}}=\mathrm{div}\left(\mathbf{T}\right)+\mathbf{R}, \tag{3}$$

where $\mathbf{T}=-p\mathbf{I}+\mu\mathbf{A}_1$ is the Cauchy stress tensor with p the isotropic pressure, $\mathbf{I}$ the identity tensor, μ the blood viscosity, and $\mathbf{A}_1$ the Rivlin Ericksen tensor. $\mathbf{R}=-\frac{\mu}{k}\mathbf{V}$ is the Darcy resistance (1856) with k the permeability of the porous medium.

The continuity and momentum equation in conservative form

$$\bar{r}\frac{\partial\bar{w}}{\partial\bar{z}}+\frac{\partial(\bar{r}\bar{u})}{\partial\bar{z}}=0, \tag{4}$$

$$\rho\left\{\frac{\partial\bar{u}}{\partial\bar{t}}+\frac{\partial\bar{u}^2}{\partial\bar{r}}+\frac{\partial\left(\bar{u}\bar{w}\right)}{\partial\bar{z}}+\frac{\bar{u}^2}{\bar{r}}\right\}=-\frac{\partial\bar{p}}{\partial\bar{r}}+\mu\left\{\frac{\partial^2\bar{u}}{\partial\bar{r}^2}+\frac{1}{\bar{r}}\frac{\partial\bar{u}}{\partial\bar{r}}+\frac{\partial^2\bar{u}}{\partial\bar{z}^2}-\frac{\bar{u}}{\bar{r}^2}\right\}-\frac{\mu}{k}\bar{u}, \tag{5}$$

$$\rho\left\{\frac{\partial\bar{w}}{\partial\bar{t}}+\frac{\partial\left(\bar{u}\bar{w}\right)}{\partial\bar{r}}+\frac{\partial\bar{w}^2}{\partial\bar{z}}+\frac{\bar{w}\bar{u}}{\bar{r}}\right\}=-\frac{\partial\bar{p}}{\partial\bar{z}}+\mu\left\{\frac{\partial^2\bar{w}}{\partial\bar{r}^2}+\frac{1}{\bar{r}}\frac{\partial\bar{w}}{\partial\bar{r}}+\frac{\partial^2\bar{w}}{\partial\bar{z}^2}\right\}-\frac{\mu}{k}\bar{w}, \tag{6}$$

and the initial and boundary conditions

$$\text{at}\ \bar{r}=0,\quad \bar{u}\left(\bar{r},\bar{z},\bar{t}\right)=0,\quad \frac{\partial\bar{w}\left(\bar{r},\bar{z},\bar{t}\right)}{\partial\bar{r}}=0, \tag{7}$$

$$\text{at}\ \bar{r}=\bar{R}\left(\bar{z},\bar{t}\right),\quad \bar{u}\left(\bar{r},\bar{z},\bar{t}\right)=\frac{\partial\bar{R}}{\partial\bar{t}},\quad \bar{w}\left(\bar{r},\bar{z},\bar{t}\right)=0, \tag{8}$$

$$\text{at}\ \bar{z}=0,\ \bar{u}\left(\bar{r},\bar{z},\bar{t}\right)=0,\ \bar{w}\left(\bar{r},\bar{z},\bar{t}\right)=\begin{cases}2U_0\left\{1-\left(\frac{\bar{r}}{\bar{R}}\right)^2\right\} & \text{for}\quad k\to\infty,\\ 2U_0\left\{\frac{I_0\left(\frac{\bar{R}}{\sqrt{k}}\right)}{I_0\left(\frac{\bar{R}}{\sqrt{k}}\right)-1}\right\}\left\{1-\frac{I_0(\bar{r}/\sqrt{k})}{I_0(\bar{R}/\sqrt{k})}\right\} & \text{for}\quad k<\infty,\end{cases} \tag{9}$$

$$\text{at}\ \bar{z}=L,\quad \frac{\partial\bar{w}\left(\bar{r},\bar{z},\bar{t}\right)}{\partial\bar{z}}=0,\quad \frac{\partial\bar{u}\left(\bar{r},\bar{z},\bar{t}\right)}{\partial\bar{z}}=0, \tag{10}$$

$$\text{at}\ \bar{t}=0,\quad \bar{u}\left(\bar{r},\bar{z},\bar{t}\right)=0,\quad \bar{w}\left(\bar{r},\bar{z},\bar{t}\right)=0,\quad \bar{p}\left(\bar{r},\bar{z},\bar{t}\right)=0,\quad \text{for}\quad \bar{z}>0, \tag{11}$$

where I_0 is the modified Bessel function of first kind and L is the length of the arterial segment considered. The axial velocity gradient and normal velocity vanishes along the axis of symmetry. The arterial wall is considered as flexible moving only in vertical direction while the longitudinal motion of the wall is neglected (Carew et al. 1968; Patel et al. 1968). Consequently, at outer boundary the axial velocity vanishes while the radial velocity is equal to the rate of wall movement. For the non-porous artery with infinite permeability, $k\to\infty$ the inlet boundary condition corresponds to the Hagen-poiseuille flow whereas in case of

artery with finite permeability $k < \infty$ the blood flow faces the Darcy's resistance for which the inlet boundary conditions (El-Shahed 2003) are derived following the same methodology adopted by Midya et al. (2003) for Hartmann flow.

Using the following dimensionless quantities

$$p = \frac{\bar{p}}{\rho U_0^2}, \quad t = \frac{U_0}{r_0}\bar{t}, \quad r = \frac{\bar{r}}{r_0}, \quad z = \frac{\bar{z}}{r_0}, \quad u = \frac{\bar{u}}{U_0},$$
$$w = \frac{\bar{w}}{U_0}, \quad R = \frac{\bar{R}}{r_0}, \quad Re = \frac{\rho U_0 r_0}{\mu}, \quad K = \frac{\rho U_0 k}{r_0 \mu}, \tag{12}$$

and the radial transformation

$$x = \frac{r}{R(z,t)}, \tag{13}$$

the Eqs. 4–6 takes the form

$$xR\frac{\partial w}{\partial z} - x^2\frac{\partial w}{\partial x}\frac{\partial R}{\partial z} + \frac{\partial (xu)}{\partial x} = 0, \tag{14}$$

$$\frac{\partial u}{\partial t} = \frac{x}{R}\frac{\partial R}{\partial z}\frac{\partial (uw)}{\partial x} - \frac{1}{R}\frac{\partial u^2}{\partial x} - \frac{\partial (uw)}{\partial z} + \frac{x}{R}\frac{\partial R}{\partial t}\frac{\partial u}{\partial x} - \frac{u^2}{xR} - \frac{1}{R}\frac{\partial p}{\partial x} + \frac{1}{ReR^2}$$
$$\times \left\{\left[1 + \left(x\frac{\partial R}{\partial z}\right)^2\right]\frac{\partial^2 u}{\partial x^2} + \left[\frac{1}{x} + 2x\left(\frac{\partial R}{\partial z}\right)^2 - xR\frac{\partial^2 R}{\partial z^2}\right]\frac{\partial u}{\partial x} + R^2\frac{\partial^2 u}{\partial z^2} - \frac{u}{x^2}\right\} - \frac{u}{K}, \tag{15}$$

$$\frac{\partial w}{\partial t} = \frac{x}{R}\frac{\partial R}{\partial z}\frac{\partial \left(w^2\right)}{\partial x} - \frac{1}{R}\frac{\partial (uw)}{\partial x} - \frac{\partial \left(w^2\right)}{\partial z} + \frac{x}{R}\frac{\partial R}{\partial t}\frac{\partial w}{\partial x} - \frac{uw}{xR} - \frac{\partial p}{\partial z} + \frac{x}{R}\frac{\partial R}{\partial z}\frac{\partial (p)}{\partial x}$$
$$+\frac{1}{ReR^2}\left\{\left[1 + \left(x\frac{\partial R}{\partial z}\right)^2\right]\frac{\partial^2 w}{\partial x^2} + \left[\frac{1}{x} + 2x\left(\frac{\partial R}{\partial z}\right)^2 - xR\frac{\partial^2 R}{\partial z^2}\right]\frac{\partial w}{\partial x} + R^2\frac{\partial^2 w}{\partial z^2}\right\} - \frac{w}{K}, \tag{16}$$

and the initial and boundary conditions (7–11) becomes

$$\text{at } x = 0, \quad u(x,z,t) = 0, \quad \frac{\partial w(x,z,t)}{\partial x} = 0, \tag{17}$$

$$\text{at } x = 1, \quad u(x,z,t) = \frac{\partial R}{\partial t}, \quad w(x,z,t) = 0, \tag{18}$$

$$\text{at } z = 0,\ u(x,z,t) = 0,\ w(x,z,t) = \begin{cases} 2\left\{1 - x^2\right\} & \text{for } K \to \infty, \\ 2\left\{\frac{I_0\left(\frac{R}{\sqrt{K}}\right)}{I_0\left(\frac{R}{\sqrt{K}}\right) - 1}\right\}\left\{1 - \frac{I_0(r/\sqrt{K})}{I_0(R/\sqrt{K})}\right\} & \text{for } K < \infty, \end{cases} \tag{19}$$

$$\text{at } z = L, \quad \frac{\partial w(x,z,t)}{\partial z} = 0, \quad \frac{\partial u(x,z,t)}{\partial z} = 0, \tag{20}$$

$$\text{at } t = 0, \quad u(x,z,t) = 0, \quad w(x,z,t) = 0, \quad p(x,z,t) = 0, \quad \text{for} \quad z > 0. \tag{21}$$

3 Numerical Method

The MAC method (Harlow and Welch 1965; Welch et al. 1966) is used to solve the highly non-linear unsteady coupled PDE's (14–16) along with the initial and boundary conditions

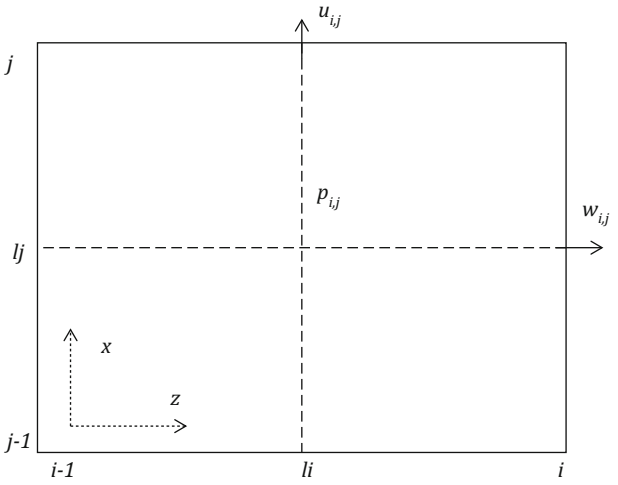

Fig. 2 MAC cell

(17–21). This method is based on finite difference scheme using staggered grid, calculates the velocities at faces while pressure at the center of the MAC cells (Fig. 2). The time derivative terms are discretized using first order accurate two-point forward time difference formula, while convective terms in the momentum equations are discretized using hybrid formula consisting of central differencing and second order upwinding. However, the diffusive terms are discretized by second order accurate three-point central difference formula. We define $x = j\Delta x, z = i\Delta z_i, t = n\Delta t$, and $p\,(x, z, t) = p^n_{i,j}$, where Δx, Δz_i represents the width, length of the (i,j)th cell and Δt refers to the time step size.

The continuity and momentum equations after discretization at (i,j)th cell takes the form

$$x_{lj}\,R_{li}\left\{\frac{w^n_{i,j}-w^n_{i-1,j}}{\Delta z_i}\right\}-x^2_{lj}\left(\frac{\partial R}{\partial z}\right)_{li}\left\{\frac{w_{at}-w_{ab}}{\Delta x}\right\}+\left\{\frac{x_j u^n_{i.j}-x_{j-1}u^n_{i.j-1}}{\Delta x}\right\}=0, \tag{22}$$

$$\left\{\frac{u^{n+1}_{i,j}-u^n_{i,j}}{\Delta t}\right\}=\frac{1}{R^n_{li}}\left\{\frac{p^n_{i,j}-p^n_{i,j+1}}{\Delta x}\right\}+(\text{ume})^n_{i,j}-\frac{u^n_{i,j}}{K}, \tag{23}$$

$$\left\{\frac{w^{n+1}_{i,j}-w^n_{i,j}}{\Delta t}\right\}=2\left\{\frac{p^n_{i,j}-p^n_{i+1,j}}{\Delta z_i+\Delta z_{i+1}}\right\}+\frac{x_{lj}}{R^n_i}\left(\frac{\partial R}{\partial z}\right)^n_i\left\{\frac{p_t-p_b}{\Delta x}\right\}+(\text{wme})^n_{i,j}-\frac{w^n_{i,j}}{K}, \tag{24}$$

where

$$\begin{aligned}
&x_{lj}=x_j-\frac{\Delta x}{2},\quad z_{li}=z_i-\frac{\Delta z_i}{2},\quad R_{li}=R(z_{li}),\\
&w_{at}=(w^n_{i,j}+w^n_{i-1,j}+w^n_{i,j+1}+w^n_{i-1,j+1})/4,\\
&w_{ab}=(w^n_{i,j}+w^n_{i-1,j}+w^n_{i,j-1}+w^n_{i-1,j-1})/4,\\
&p_t=\left\{\left(p^n_{i,j}+p^n_{i,j+1}\right)\Delta z_{i+1}+\left(p^n_{i+1,j}+p^n_{i+1,j+1}\right)\Delta z_i\right\}/2\{\Delta z_{i+1}+\Delta z_i\},\\
&p_b=\left\{\left(p^n_{i,j}+p^n_{i,j-1}\right)\Delta z_{i+1}+\left(p^n_{i+1,j}+p^n_{i+1,j-1}\right)\Delta z_i\right\}/2\{\Delta z_{i+1}+\Delta z_i\},
\end{aligned} \tag{25}$$

$$(\text{ume})^n_{i,j} = \text{Con}(u)^n_{i,j} + \frac{1}{Re}(\text{Diff}(u)^n_{i,j}),$$
$$(\text{wme})^n_{i,j} = \text{Con}(w)^n_{i,j} + \frac{1}{Re}\left(\text{Diff}\,(w)^n_{i,j}\right), \tag{26}$$

where $\text{Con}(u)^n_{i,j}$ and $\text{Con}(w)^n_{i,j}$ are convective terms while $\text{Diff}(u)^n_{i,j}$ and $\text{Diff}(w)^n_{i,j}$ are diffusive terms for u and w-momentum equation and at the nth time level at the (i, j) cell, respectively.

The radial and axial momentum equations are used in the continuity equation to obtain the Poisson equation for pressure. The final form of the Poisson equation is

$$\begin{aligned}\left\{\frac{\text{Div}^{n+1}_{i,j} - \text{Div}^n_{i,j}}{\Delta t}\right\} &= A_{i,j}\,p^n_{i,j} + B_{i,j}\,p^n_{i+1,j} + C_{i,j}\,p^n_{i-1,j} + D_{i,j}\,p^n_{i,j+1}\\ &+E_{i,j}\,p^n_{i,j-1} + F_{i,j}\,p^n_{i+1,j+1} + G_{i,j}\,p^n_{i+1,j-1} + H_{i,j}\,p^n_{i-1,j-1}\\ &+I_{i,j}\,p^n_{i-1,j+1} + x_{lj}\,R_{li}\left\{\frac{(\text{wme})^n_{i,j} - (\text{wme})^n_{i-1,j}}{\Delta z_i}\right\}\\ &+\left\{\frac{x_j\,(\text{ume})^n_{i.j} - x_{j-1}(\text{ume})^n_{i.j-1}}{\Delta x}\right\} - x_{lj}\,R_{li}\left\{\frac{w^n_{i,j} - w^n_{i-1,j}}{K\,\Delta z_i}\right\}\\ &-\left\{\frac{x_j\,u^n_{i.j} - x_{j-1}u^n_{i.j-1}}{K\,\Delta x}\right\},\end{aligned} \tag{27}$$

Here, $\text{Div}^k_{i,j}$ represents the divergence of velocity field at the (i, j) cell. The Poisson equation for pressure is then solved iteratively by the Successive-Over-Relaxation (SOR) method with a certain number of iterations to get the intermediate pressure field at the nth time step. To increase the rate of convergence the value of over-relaxation parameter is taken, 1.2.

3.1 Pressure and Velocity Corrections

Since, the pressure obtained after solving the pressure equation is intermediate so the resulting velocity will not satisfy the continuity equation. To calculate the correct velocity, we use the pressure correction relation

$$p^n_{i,j} = \bar{p}_{i,j} + \alpha\,\Delta p_{i,j}, \tag{28}$$

where $\bar{p}_{i,j}$ is intermediate pressure after solving the pressure equation, $\alpha, 0 < \alpha < 0.5$ is the under relaxation parameter and $\Delta p_{i,j}$ is the pressure error term given by

$$\Delta p_{i,j} = -\frac{\overline{\text{Div}}_{i,j}}{\Delta t\,A_{i,j}}, \tag{29}$$

where $\overline{\text{Div}}_{i,j}$ is the divergence of intermediate velocity. The velocity correction formulas are

$$w^{n+1}_{i,j} = \bar{w}_{i,j} + \frac{2\Delta t\,\Delta p_{i,j}}{(\Delta z_i + \Delta z_{i+1})}, \tag{30}$$
$$u^{n+1}_{i,j} = \bar{u}_{i,j} + \frac{\Delta t\,\Delta p_{i,j}}{R_{li}\,\Delta x}, \tag{31}$$

where $\bar{w}_{i,j}$ and $\bar{u}_{i,j}$ are the intermediate velocity components obtained using intermediate pressure.

3.2 Stability Restriction and Numerical Scheme

The step-by-step time interval is chosen as suggested by Welch et al. (1966) and Amsden and Harlow (1970) to reduce the running time. The first stability condition is adopted from Welch et al. (1966) which depends upon Reynolds number and spatial step size

$$\Delta t_1 \leq \text{Min}\left(\frac{Re\Delta x^2 \Delta z_i^2}{2(\Delta x^2 + \Delta z_i^2)}\right)_{i,j}. \tag{32}$$

The second condition used by Markham and Proctor (1983) which requires that no particles should cross more than one cell boundary in a given time interval.

$$\Delta t_2 \leq \text{Min}\left(\frac{\Delta z_i}{|w|}, \frac{\Delta x}{|w|}\right)_{i,j}. \tag{33}$$

In view of both the conditions the stability condition is taken as

$$\Delta t = \gamma \text{Min}\left(\Delta t_1, \Delta t_2\right)_{i,j}, \tag{34}$$

where γ, $0 < \gamma < 1$ is used to save the computation time as evident from Markham and Proctor (1983). Moreover, the upwinding parameter β is selected as

$$1 > \beta > \text{Max}\left(\left|\frac{w\Delta t}{\Delta z_i}\right|, \left|\frac{u\Delta t}{\Delta x}\right|\right)_{i,j}. \tag{35}$$

This inequality yields a very small value of the parameter β. As a safety measure the value is multiplied by a factor 1.2.

For numerical computations, the arterial segment has been confined to 60 times the non-dimensional radius. To avoid any distortion in the beginning of stenoses and inlet boundary condition the upstream arterial length is taken to be eight radii and downstream length is taken ten radii to re-establish the fully developed flow. Also, the couple of stenoses is separated by the two radii non-stenotic arterial segment. For this computational domain, solutions are computed on the staggered grids with 39,160 grid elements. The finer mesh is obtained by interpolating the experimental data of Back et al. (1984). The physiological range of mean Reynolds number is 100–400 for blood flow through healthy main coronary artery (Back and Banerjee 2000) but in case of diseased state like stenosed artery or blood flow with anemia (lower hematocrit), the Reynolds number becomes high resulting turbulent blood flow. So, in this problem, $Re =$ 450 and 1,000 are chosen for the study of blood flow in multi-irregular-diseased stenosed artery. The numerical values of permeability parameter K are chosen following Dash et al. (1996) and El-Shahed (2003) which represent different ratios for the porous medium while the numerical values of other involving parameters are taken within the physiological range (Mekheimer and Kot 2008; Johnson et al. 1992; McDonald 1974) as follows:

$$\rho = \frac{1050\,\text{kg}}{\text{m}^3}, \quad \omega = 2\pi f_\text{p}, \quad f_\text{p} = 1.2\,\text{Hz}, \quad \phi = 0, \quad \Delta x = 0.025.$$

4 Discussions

The numerical simulation is performed for governing equations and the numerical solutions are calculated under physiological flow conditions. The results presented are obtained after

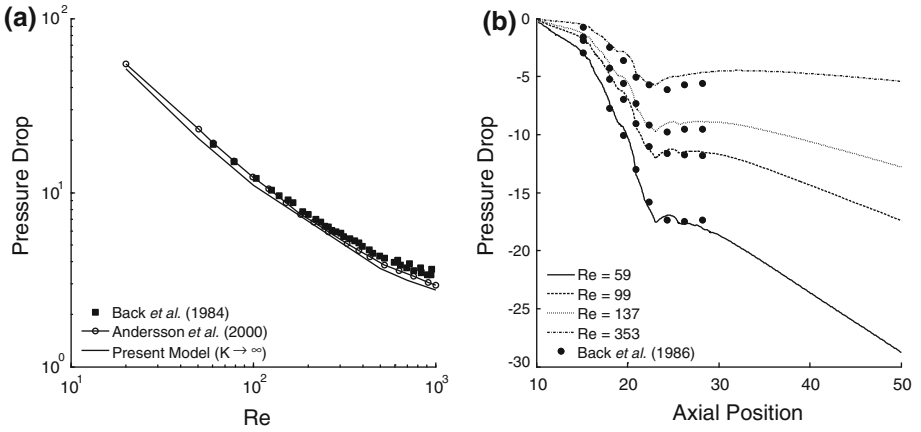

Fig. 3 Comparisons of pressure drop for present model ($K \rightarrow \infty$) with single stenoses

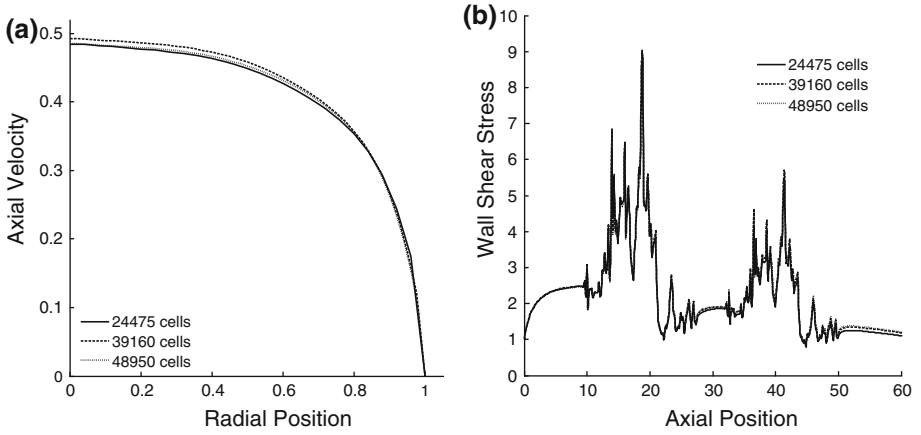

Fig. 4 Grid independence analysis for **a** axial velocity profile at $z = 18.85$ and **b** wall shear stress for different grid size with fixed $K = 10$ and $Re = 1{,}000$

the steady state achieved in the simulation. The effects of permeability parameter K and Reynolds number Re on the pressure drop, velocity profiles, separation zones, re-circulation regions, and vorticity are examined graphically to investigate the influence of constricted geometry and porous media on blood rheology.

4.1 Model Validation

To assure the validity of this model, the results for pressure drop calculated for single stenoses in non-porous artery ($K \rightarrow \infty$) are compared with the experimental results of Back et al. (1984), Back et al. (1986), and numerical results of Andersson et al. (2000). The comparisons for pressure drop versus Reynolds number and axial position are presented in Fig. 3a, b, respectively. These results clearly depict a close agreement between predicted pressure drop and experimentally measured pressure drop (Back et al. 1984, 1986) with a slight deviation which is due to the unsteadiness of flow, different mesh size, and other factors involved. These

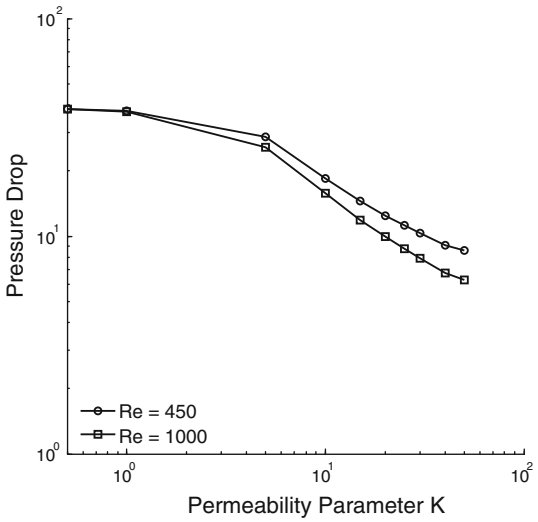

Fig. 5 Pressure drop against permeability parameter K for $Re = 450$ and 1,000

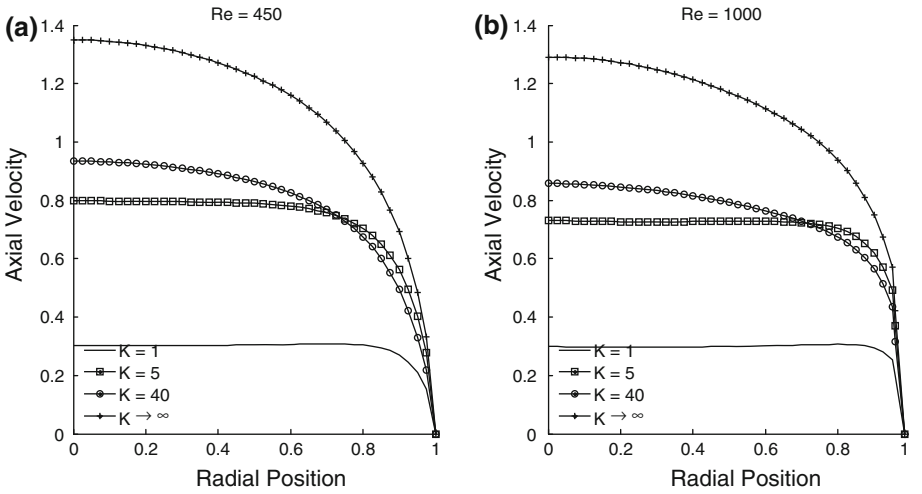

Fig. 6 Axial velocity profile against radial position for different K at cross section $z = 18.85$

comparisons are followed by the study of Yakhot et al. (2005) and Johnston and Kilpatrick (1991).

To verify this model, the grid independence study is accomplished for velocity and wall shear stress. A number of numerical simulations are performed for different time step and grid size for refined mesh with 24475, 39160, and 48950 MAC cells. The axial velocity profiles at the point of maximum constriction for these cases are shown in Fig. 4a while wall shear stress for different meshes is presented in Fig. 4b with fixed $K = 10$ and $Re = 1000$. It can be seen clearly that the velocity profiles and wall shear stress are almost overlapping for different mesh size. This analysis is done to examine the measure of error related with different grid size; the error found is of negligible order which assures the correctness of the solutions obtained.

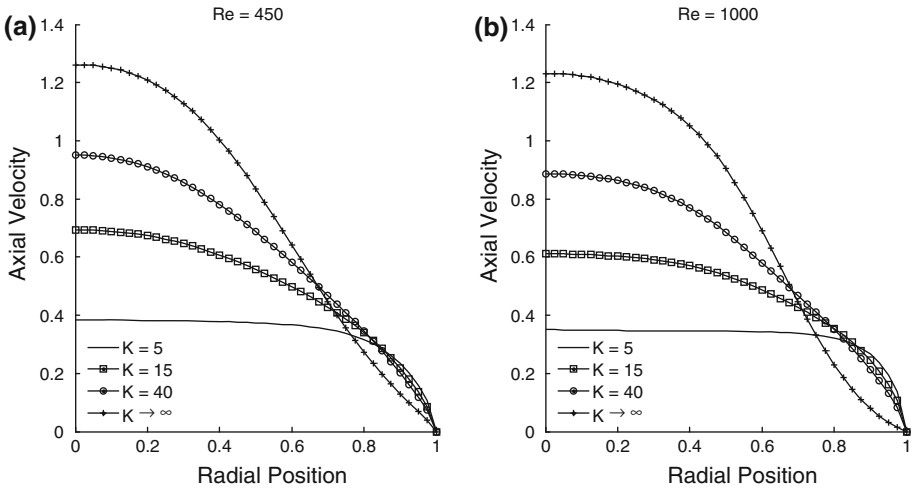

Fig. 7 Axial velocity profile against radial position for different K at cross section $z = 30$

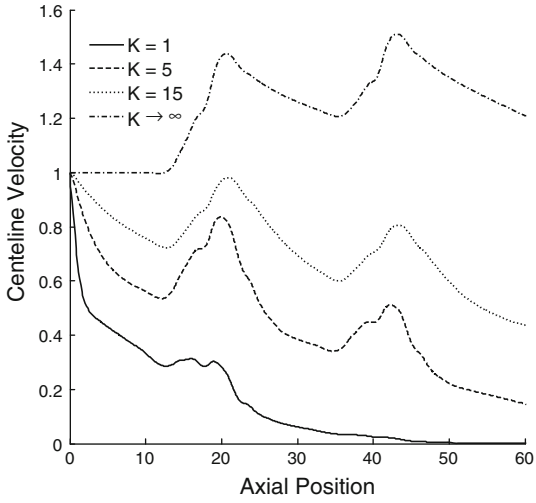

Fig. 8 Centerline velocity against axial position for different K at $Re = 450$

4.2 Mild Stenoses

The dimensionless pressure drop against the permeability parameter K is plotted in Fig. 5 for different Re. It is noticed that pressure drop decreases with the increase in permeability parameter. This decrease in pressure drop becomes sharp for larger values of the permeability parameter. It is also seen that the pressure drop is a decreasing function of Reynolds number.

Figures 6 and 7 illustrate the effects of permeability parameter on axial velocity profile against radial direction at the point of maximum constriction ($z = 18.85$) of the proximal stenoses and in the unstenosed region ($z = 30$), respectively. It is observed that the velocity profile is in increasing trend for increasing permeability parameter. The reason for this behavior is may be the decrease in resistance (for increasing permeability) provided by the porous medium. It is also observed that for infinite permeability the velocity profile is almost

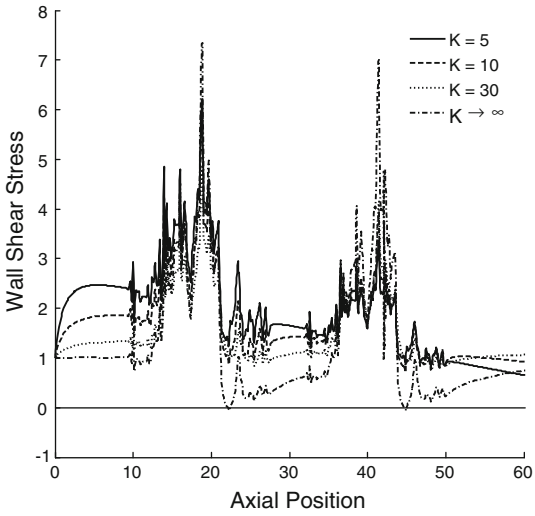

Fig. 9 Wall shear stress for different values of K at $Re = 450$

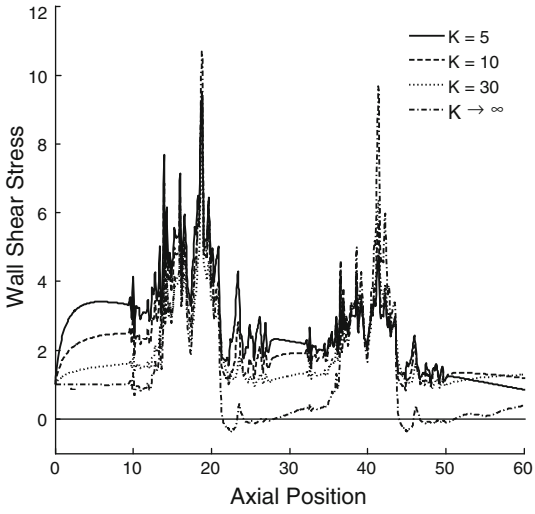

Fig. 10 Wall shear stress for different values of K at $Re = 1{,}000$

parabolic which becomes steeper on decreasing the permeability of the medium. The results are in quite good agreement with Dash et al. (1996). The comparison of Figs. 6 and 7 shows that the magnitude of velocity is larger at the point of maximum constriction when compared to the velocity in the unstenosed artery. The centerline velocity is plotted with axial coordinate for different values of permeability parameter in Fig. 8. The centerline velocity decreases for decreasing permeability parameter. It is worth to mention that for small permeability parameter ($K = 1$) the centerline velocity diminishes and the blood flow reaches to the stationary state.

The points where the shear stress at the wall becomes zero or changes its sign are termed as flow separation points. Followed by the flow separation points, the reattachment points exist when the shear stress at the wall changes its sign again. The region between the flow separation point and the reattachment point is characterized as flow separation region or separation

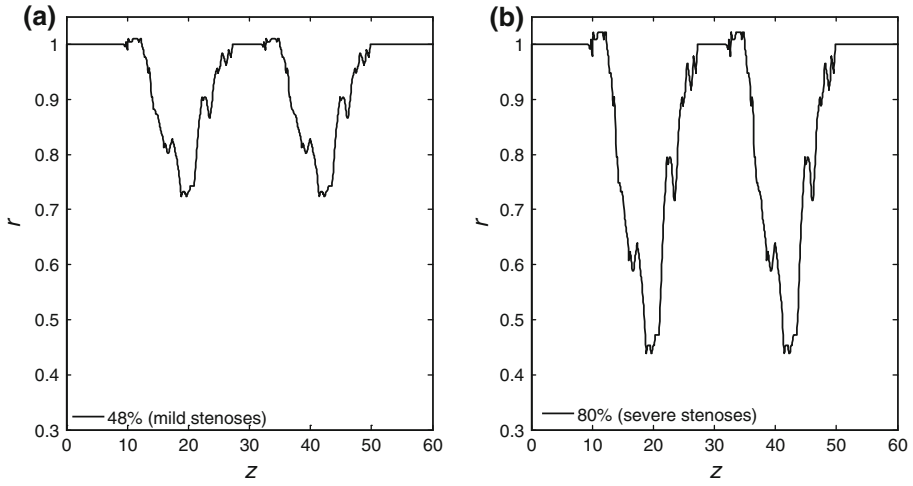

Fig. 11 Original stenoses with 48% areal occlusion and modified stenoses with 80% areal occlusion

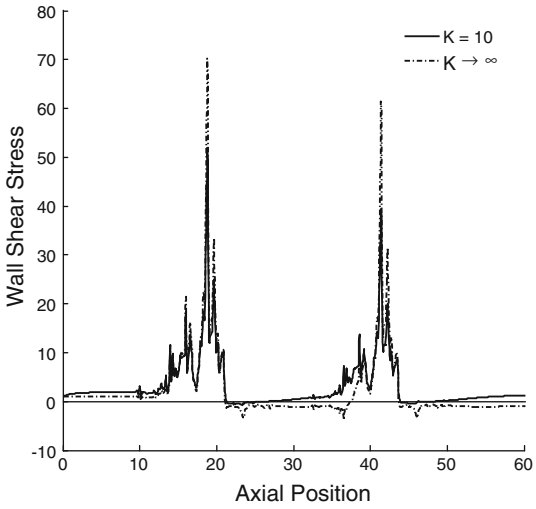

Fig. 12 Wall shear stress for different K with severe (80%) stenoses at $Re = 450$

zone. For mild (48%) stenoses, the wall shear stress distribution for different values of permeability parameter is presented in Figs. 9 and 10 for $Re = 450$ and 1,000. It is observed that for increasing permeability parameter wall shear stress distribution decreases but the peak values of wall shear stress distribution increases at the points of severe stenoses in the arterial segment. No separation zones are found for finite permeability parameter. Moreover, for infinite permeability, the critical value of Reynolds number for which the separation zones are found along the downstream of both stenoses is $Re = 450$ and for $Re = 1{,}000$ quite large separation zone are found in the downstream of both stenoses.

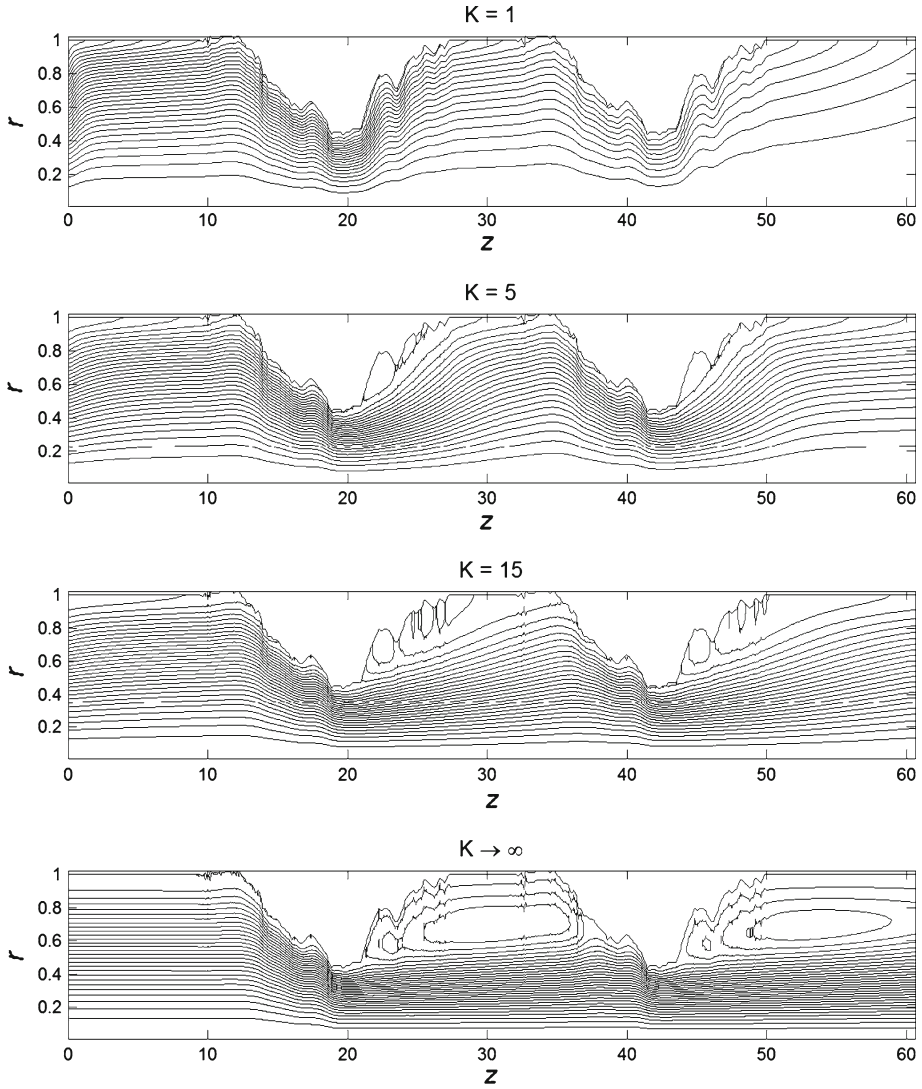

Fig. 13 Stream line patterns with 80% areal occlusion at $Re = 450$ for different K

4.3 More Severe Stenoses

The original experimental data of Back et al. (1984) is with 48% areal occlusion having mild stenoses. This data is modified to obtain the severe stenoses with 80% areal occlusion maintaining the original shape of stenoses with similar irregularities. This modification is made, to further investigate the separation zones, re-circulation regions and vorticity contours for severe stenoses. The geometry of mild and severe stenoses is presented in Fig. 11.

Figure 12 is plotted to examine the effects of severe stenoses (80%) on flow separation both in case of porous and non-porous medium. For this reason, wall shear stress distribution is sketched for different permeability parameter $K = 10$ and $K \to \infty$ with Reynolds number

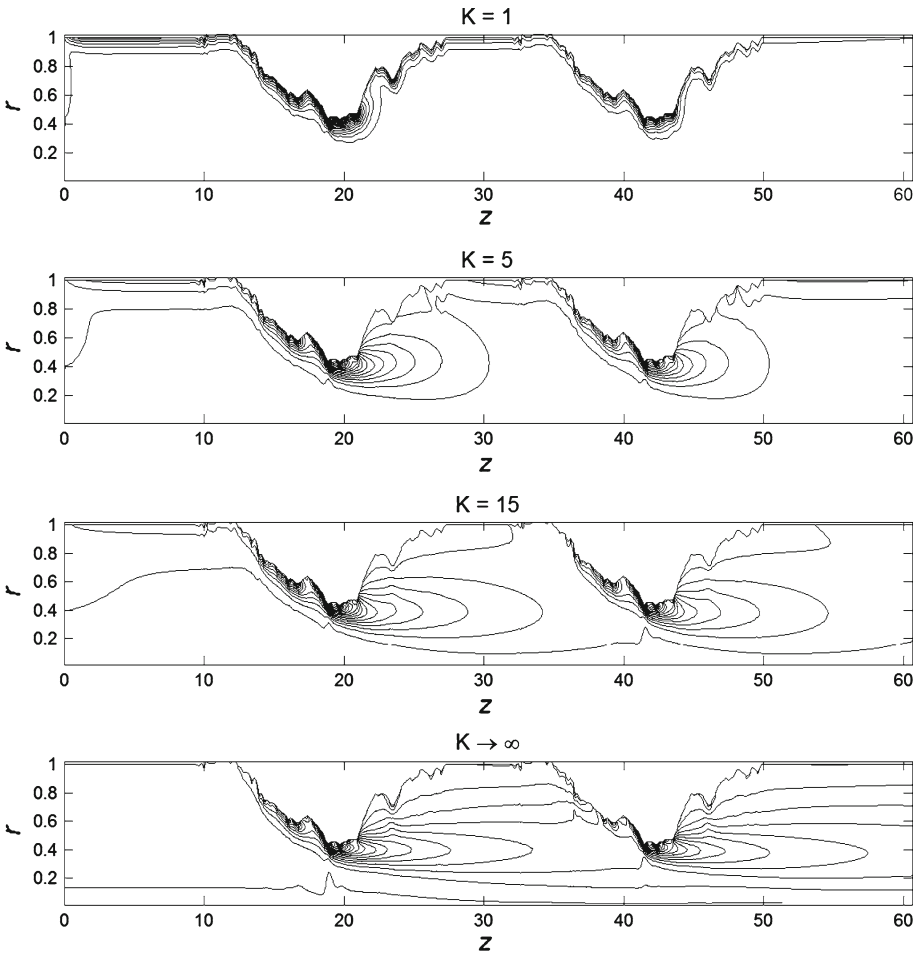

Fig. 14 Vorticity contours with 80% areal occlusion at $Re = 450$ for different K

of 450 under 80% areal occlusion. This Fig. 12 depicts that for non-porous medium, large separation zones are found in the downstream of both stenoses. Moreover, it is worth to mention that in case of porous medium, although small, but separation zones are seen across both stenoses as those were not seen in case of mild stenoses (Figs. 9, 10).

The stream line patterns for different values of permeability parameter with $Re = 450$ and 80% areal occlusion are exhibited in Fig. 13. The large re-circulation regions are found in the downstream of both stenoses for infinite permeability parameter. These re-circulation regions reduce with decreasing permeability parameter. Further, for small permeability ($K = 1$) the re-circulation regions completely disappear. Figure 14 records the behavior of vorticity contours for permeability parameter with 80% areal occlusion. It is noticed that in non-porous medium ($K \to \infty$) the tortuous vorticity contours are found adjacent to maximum point of constriction. These contours move toward the centerline as the mean flow decelerates. For decreasing permeability parameter these contours diminishes and furthermore these contours disappear completely for small permeability parameter ($K = 1$). These results are compatible

with those found in Figs. 12 and 13 i.e., the reduction of separation zone and recirculation region with the decrease in permeability parameter.

5 Conclusions

This attempt is devoted to the study of blood flow in a 2D unsteady axisymmetric-diseased porous arterial segment with a couple of constrictions with real surface irregularities. The governing equations are solved numerically using MAC method following finite difference scheme. The grid independence study is performed to verify the model and comparisons with existing experimental and numerical work is presented. This model will be helpful particularly in the study of diseased arterial blood flow when the artery contains the thrombus, cholesterol, fatty plaques, etc. The following results are noted:

- The mathematical model is independent of the grid size and time step.
- Pressure drop decreases with increasing permeability parameter.
- The velocity profile entirely depends upon the permeability of the medium, smaller permeability highly decelerates the flow.
- Wall shear stress is a decreasing function of permeability parameter. For mild (48%) stenoses, no separation zones are found whereas, although, small separation zones are found for severe (80%) stenoses in case of porous medium.
- The re-circulation/eddy and vortex contours exist in the downstream of each stenoses in non-porous artery which diminishes with the decreasing permeability of the porous medium.

Acknowledgments The authors would like to acknowledge Ministry of Higher Education (MOHE) and Research Management Centre—UTM for the financial support through vote numbers Q. J130000.7126.03J54 and 78528 for this research.

References

Ai, L., Vafai, K.: A coupling model for macromolecule transport in a stenosed arterial wall. Int. J. Heat Mass Transf. **49**, 1568–1591 (2006)

Amsden, A.A., Harlow, F.H.: The SMAC method: a numerical technique for calculating incompressible fluid flow. Los Alamos Scientific Lab. Report LA-4370, LosAlamos (1970)

Andersson, H.I., Halden, R., Glomsaker, T.: Effects of surface irregularities on flow resistance in differently shaped arterial stenoses. J. Biomech. **33**, 1257–1262 (2000)

Back, L.H., Banerjee, R.K.: Estimated flow resistance increase in a spiral human coronary artery segment. J. Biomech. Eng. **122**, 675–677 (2000)

Back, L.H., Cho, Y.I., Crawford, D.W., Cuffel, R.F.: Effect of mild atherosclerosis on flow resistance in a coronary artery casting of man. ASME J. Biomech. Eng. **106**, 48–53 (1984)

Back, L.H., Radbill, J.R., Cho, Y.I., Crawford, D.W.: Measurement and prediction of flow through a replica segment of a mildy atherosclerotic coronary artery of a man. J. Biomech. **19**, 1–17 (1986)

Baish, J.W., Netti, P.A., Jain, R.K.: Transmural coupling of fluid flow in microcirculatory network and interstitium in tumors. Microvasc. Res. **53**, 128–141 (1997)

Carew, T.E., Vaishnav, R.N., Patel, D.J.: Compressibility of the arterial wall. Circ. Res. **23**, 61–68 (1968)

Darcy, H.R.P.G.: Les Fontaines Publiques de la volle de Dijon. Vector Dalmont, Paris (1856)

Dash, R.K., Mehta, K.N., Jayaraman, G.: Casson fluid flow in a pipe filled with a homogeneous porous medium. Int. J. Eng. Sci. **34**, 1145–1156 (1996)

El-Shahed, M.: Pulsatile flow of blood through a stenosed porous medium under periodic body acceleration. Appl. Math. Comput. **138**, 479–488 (2003)

Harlow, F., Welch, J.E.: Numerical calculation of time-dependent viscous incompressible flow of fluid with free surface. Phys. Fluids. **8**, 2182–2189 (1965)

Jeong, W.W., Rhee, K.: Effects of surface geometry and non-Newtonian viscosity on the flow field in arterial stenoses. J. Mech. Sci. Technol. **23**, 2424–2433 (2009)
Johnson, G.A., Borovetz, H.S., Anderson, J.L.: A model of pulsatile flow in uniform deformable vessel. J. Biomech. **25**, 91–100 (1992)
Johnston, P.R., Kilpatrick, D.: Mathematical modelling of flow through an irregular arterial stenoses. J. Biomech. **24**, 1069–1077 (1991)
Khakpour, M., Vafai, K.: Critical assessment of arterial transport models. Int. J. Heat Mass Transf. **51**, 807–822 (2008)
Khakpour, M., Vafai, K.: Effects of gender-related geometrical characteristics of aorta–iliac bifurcation on hemodynamics and macromolecule concentration distribution. Int. J. Heat Mass Transf. **51**, 5542–5551 (2008)
Khaled, A.R.A., Vafai, K.: The role of porous media in modeling flow and heat transfer in biological tissues. Int. J. Heat Mass Transf. **46**, 4989–5003 (2003)
Lei, X.X., Wu, W.Y., Wen, G.B., Chen, J.G.: Mass transport in solid tumors (I)—fluid dynamics. Appl. Math. Mech. Eng. Ed. **19**, 1025–1032 (1998)
Liepsch, D.: An introduction to biofluid mechanics: basic models and applications. J. Biomech. **35**, 415–435 (2002)
Markham, G., Proctor, M.V.: Modifications to the two-dimensional incompressible fluid flow code ZUNI to provide enhanced performance, C.E.G.B. Report TPRD/L/0063/M82 (1983)
McDonald, D.A.: Blood Flow in Arteries, 2nd ed. Edward Arnold, London (1974)
Mekheimer, Kh.S., Kot, M.A.El.: Influence of magnetic field and hall currents on blood flow through a stenotic artery. Appl. Math. Mech. **29**, 1093–1104 (2008)
Midya, C., Layek, G.C., Gupta, A.S., Mahapatra, T.R.: Magnetohydrodynamic viscous flow separation in a channel with constrictions. ASME J. Fluid Eng. **125**, 952–962 (2003)
Milosevic, M.F., Fyles, A.W., Hill, R.P.: The relationship between elevated interstitial fluid pressure and blood flow in tumors: a bioengineering analysis. Int. J. Radiat. Oncol. Biol. Phys. **43**, 1111–1123 (1999)
Mustapha, N., Mandal, P.K., Johnston, P.R., Amin, N.: A numerical simulation of unsteady blood flow through multi-irregular arterial stenoses. Appl. Math. Model. **34**, 1559–1573 (2010)
Nerem, R.M., Seed, W.A.: An in vivo study of aortic flow disturbances. Cardiovasc. Res. **106**, 1–14 (1972)
Patel, D.J., Greenfield, J.C, Fry, D.L.: In vivo pressure–length–radius relationship of certain blood vessels in man and dog. In: Attinger, E.O. (ed.) Pulsatile Blood Flow, pp. 293–302. McGraw-Hill, New York (1968)
Srivastava, V.P., Saxena, M.: Suspension model for blood flow through stenotic arteries with a cell-free plasma layer. Math. Biosci. **139**, 79–102 (1997)
Srivastava, V.P., Rastogi, R., Vishnoi, R.: A two-layered suspension blood flow through an overlapping stenoses. Comput. Math. Appl. **60**, 432–441 (2010)
Sud, V.K., Sekhon, G.S.: Flow through a stenosed artery subject to periodic body acceleration. Med. Biol. Eng. Comput. **25**, 638–644 (1987)
Welch, J.E., Harlow, F.H., Shannon, J.P., Daly, B.J.: The MAC Method, Los Alamos Scientific Lab, Report LA-3425, Los Alamos (1966)
Yakhot, A., Grinberg, L., Nikitin, N.: Modelling rough stenoses by an immersed-boundary method. J. Biomech. **38**, 1115–1127 (2005)
Yang, N., Vafai, K.: Modeling of low-density lipoprotein (LDL) transport in the artery—effects of hypertension. Int. J. Heat Mass Transf. **49**, 850–867 (2006)
Yang, N., Vafai, K.: Low-density lipoprotein (LDL) transport in an artery—a simplified analytical solution. Int. J. Heat Mass Transf. **51**, 497–505 (2008)
Young, D.F.: Effect of a time dependant stenoses on flow through a tube. J. Eng. Ind. Trans. ASME **90**, 248–254 (1968)